Desalination and Water Treatment
www.deswater.com
doi: 10.1080/19443994.2013.817533

52 (2014) 6219–6229
September

Taylor & Francis
Taylor & Francis Group

Evaluation of removal efficiency of fluoride from aqueous solution using nanosized fluorapatite

Wei Wei[a], Xue Wang[a,b], Yu Wang[c], Min Xu[a], Jing Cui[a], Zhenggui Wei[a,*]

[a]*Department of Environmental Science and Engineering, Nanjing Normal University, Nanjing 210046, P.R. China*
Tel./Fax: +86 25 8439 5014; email: weizhenggui@gmail.com
[b]*College of Chemistry and Materials Science, Nanjing Normal University, Nanjing 210023, China*
[c]*School of Resources and Environment, Anqing Teachers College, Anqing 246011, China*

Received 23 February 2012; Accepted 30 May 2013

ABSTRACT

In this study, the potential of nanosized fluorapatite (*n*FAP) for fluoride removal from aqueous solution was evaluated. Several parameters including adsorbent dosage, contact time, initial fluoride concentration and pH were investigated for their effects on the removal of fluoride. A detailed analysis of the regression coefficients showed that Langmuir and Freundlich models adequately described the adsorption data, but the data were better fitted by the Langmuir isotherm. While the pseudo-second-order model was the best choice to describe the fluoride adsorption behavior, and thermodynamic studies revealed that the adsorption of flouride by *n*FAP was spontaneous and endothermic in nature. *n*FAP exhibited a great defluoridation capacity up to 7.45 mg/g, which was similar to that of nanosized hydroxyapatite (7.75 mg/g). In consideration of the lower cost and easier regeneration property of *n*FAP, it would provide an alternative for the adsorption and removal of fluoride from aqueous solution.

Keywords: Nanosized fluorapatite; Adsorption; Aqueous solution; Fluoride

1. Introduction

Extensive research has been carried out on the removal of fluoride from aqueous solution because of the adverse effect it has on the human body [1–3]. Various defluoridation technologies have been developed to reduce the fluoride concentration in water, such as adsorption [4,5], ion exchange [6,7], precipitation [8,9], and membrane process [10,11]. Among these methods, adsorption process is the most widely used for the removal of fluoride. This is due to its easy operational procedure and cost-effectiveness [12]. Many naturally occurring minerals have been tested for possible use as adsorbents, especially apatite family minerals, such as phosphate rock (PR, main component is fluorapatite) [13], hydroxyapatite (HAP) [14], and nanosized hydroxyapatite (*n*HAP) [12,15–17].

In recent years, great progress has been made in the study of fluoride removal with apatite family minerals. For example, Gao et al. have studied the size-dependant defluoridation properties of synthetic

*Corresponding author.

HAP and have drawn a conclusion that the smaller the particle size, the better the fluoride adsorption capacity [16]. This result could be explained by the different defluoridation mechanisms of HAP with various particle sizes. It is generally considered that the removal of fluoride by HAP is based on an ion exchange process, in which fluoride ions partly or entirely exchange with hydroxyl group of HAP [12]. While, it was found that the adsorption of fluoride by *n*HAP was mainly through the formation of O–H···F hydrogen bond as reported by Sairam Sundaram et al. [18] and Wang et al. [17]. Furthermore, through hydrogen bonding, *n*HAP exhibited a great defluoridation capacity up to 7.605 mg/g [17], which was much better than bulk apatite materials, such as PR and HAP. Therefore, *n*HAP is an excellent adsorbent for the removal of fluoride. However, the relatively high cost and the difficulties associated with its regeneration restrict the application of *n*HAP in defluoridation. In order to overcome the drawbacks of *n*HAP and achieve excellent defluoridation efficiency by hydrogen bonding, we devote to the study of nanosized fluorapatite (*n*FAP) as adsorbents for the fluoride removal instead of *n*HAP. Fluorapatite (FAP) is a natural mineral with the formula $Ca_{10}(PO_4)_6F_2$, and it occurs widely as an accessory mineral in igneous rocks and in calcium rich metamorphic rocks. Meanwhile, *n*FAP could be obtained by simple and cost-effective mechanical grinding of FAP. Previous study also showed that *n*HAP would transform into F-substituted HAP or FAP after several adsorption processes [14]. Therefore, studying the fluoride removal efficiency by *n*FAP is also a research for the regeneration of *n*HAP.

The objectives of this paper are to evaluate that if *n*FAP has the same defluoridation efficiency as *n*HAP, and to find out if the regeneration of *n*FAP has better performance compared with *n*HAP.

2. Materials and methods

2.1. Materials

All reagents used in this work were of analytical grade and supplied by Nanjing Chemical Reagent Company. The chemicals used in the synthesis process were $Ca(NO_3)_2{\cdot}4H_2O$, $(NH_4)_2HPO_4$, NH_4F and a solution of 35% ammonia. NaF was used to prepare the 1,000 mg/L fluoride stock solution, which was then used to prepare the diluted solution for each of the batch adsorption studies. Total ionic strength adjusting buffer (TISAB-III) solution was added to both the samples and standards in the ratio of 1:10.

2.2. Synthesis and characterization of adsorbents

*n*HAP, *n*FHAP, and *n*FAP were synthesized by solution-precipitation method. Calcium nitrate 4-hydrate ($Ca(NO_3)_2{\cdot}4H_2O$), diammonia hydrogen phosphate ($(NH_4)_2HPO_4$), and ammonia fluoride (NH_4F) were used as the precursors for Ca^{2+}, PO_4^{3-}, and F^-, respectively, and ammonia solution is used as agents for pH adjustment. Synthesis of pure HAP involved the reaction of $Ca(NO_3)_2{\cdot}4H_2O$ and $(NH_4)_2HPO_4$ with a Ca/P ratio close to 1.67. $Ca(NO_3)_2{\cdot}4H_2O$ dissolved in distilled water was vigorously stirred on a beaker to form a 0.24 mol/L solution, and a $(NH_4)_2HPO_4$ of 0.29 mol/L was slowly added dropwise to the $Ca(NO_3)_2{\cdot}4H_2O$ solution. 50% F-substituted HAP ($Ca_{10}(PO_4)_6FOH$, *n*FHAP) and pure fluorapatite *n*FAP ($Ca_{10}(PO_4)_6F_2$) were prepared assuming that F^- ions would substitute for the hydroxide site in the *n*HAP lattice. During these stir processes, the pH level should be brought to 11, and all precipitates had been removed from solution by centrifugation method at the rotation speed of 4,000 rpm, and the powder was dried at 100°C [19].

Fluoride content in both *n*FAP and *n*FHAP were determined by using a fluoride-selective electrode in total ionic strength adjusting buffer solution. In 10 mL of 1 M nitric acid, 0.1 g of each sample was dissolved and then diluted by 100 mL of deionized water. Standard solutions made from NaF were used to calibrate the measurement in the same buffer solution. FTIR spectral investigations were carried out using a Tensor 27 FTIR spectrometer. The KBr pellet technique was used and the spectra data were recorded from 4,000 to 400 cm^{-1} with a resolution of 4 cm^{-1}. The phase purity and crystallinity of the synthetic samples were determined by powder X-ray diffraction (XRD) using Cu Kα ($\lambda = 1.5405$ Å) radiation on a Rigaku D/max-IIIB X-ray powder diffractometer. The morphology and size of the synthetic nanosized adsorbents were characterized by a Hitachi Model H-7650 transmission electron microscope.

2.3. Adsorption experiments

Batch adsorption experiments were carried out by mixing 0.1 g adsorbent added to 25 mL of solution containing 10 mg/L as initial fluoride concentration at pH 5.0. The contents were shaken thoroughly using a magnetic stirrer at a speed of 200 rpm for 120 min and then by centrifugation for 15 min at 25°C. Then, the suspensions were centrifuged and filtered, and the residual fluoride was measured immediately by pH/ISE meter (Orion 148 Model, EA 940 Expandable Ion Analyzer). The adsorption studies have been

carried out with varying pH adjusted with 0.1 mol/L NaOH or 0.1 mol/L HCl. The kinetic studies of the adsorption were carried out at a constant temperature of 25°C. The thermodynamic parameters of the adsorption were established by conducting the experiments at 25, 35, 45, and 55°C in a temperature controlled mechanical shaker.

The removal efficiency of fluoride was calculated from the equation below:

$$\% \text{ Removal} = (C_0 - C_e)/C_0 \times 100$$

The defluoridation capacity q_e was calculated from the following mass balance equation:

$$q_e = (C_0 - C_e)\ V/m$$

where q_e (mg/g) is the equilibrium adsorption capacity; C_0 and C_e (mg/L) are the initial and equilibrium concentrations of fluoride in solution; m and V are adsorbent mass and the volume of the contaminated solution, respectively. All the adsorption experiments above were conducted in triplicate and it was found that the errors for all tests were ± 5%. Therefore, the average values of the three tests were used as adsorption data.

2.4. Desorption experiments

The recycling of an adsorbent is the most important aspect for an economical technology. For this purpose, desorption studies were carried out by using the fluoride-adsorbed adsorbents (*n*HAP, *n*FHAP, and *n*FAP). First, the fluoride-adsorbed adsorbent was generated by adsorbing 10 mg/L fluoride solution on 4 g/L adsorbent at pH 5.0. After the equilibration, the residue was filtered and the filtrate was measured for fluoride content. Then, this fluoride-adsorbed adsorbent was subjected for desorption studies by adding different concentrations of NaOH (0.2–1.5 g/L). The suspensions were then shaken at 25°C for about 120 min and filtered, after which the filtrates were adjusted to pH 6.0–7.0 with 0.45 mol/L H_2SO_4 and fluoride amount desorbed into the solutions were determined to calculate removal extent (percent).

3. Results and discussion

3.1. Characterization of adsorbents

Fluoride content in both *n*FAP and *n*FHAP was determined by using a fluoride-selective electrode and the results are given in Table 1. As indicated in this table, fluoride content in the synthetic *n*FAP is close to the theoretical fluoride content of pure fluorapatite, and the synthetic *n*FHAP is 50% F-substituted HAP.

Table 1
Fluoride content in the synthetic adsorbents (*n*HAP, *n*FHAP, and *n*FAP)

Sample	Formula	Fluoride, wt.%	
		Nominal	Actual
*n*HAP	$Ca_{10}(PO_4)_6(OH)_2$	0	0
*n*FHAP	$Ca_{10}(PO_4)_6FOH$	1.89	1.84
*n*FAP	$Ca_{10}(PO_4)_6F_2$	3.77	3.52

According to the TEM (Fig. 1), the synthesized *n*HAP, *n*FHAP, and *n*FAP are about 50–60 nm with cylindrical rod like shape. It is clear that the particles are of homogeneous microstructure and formed a uniform nanomaterial [20].

The mineralogical identity of adsorbent particles was verified by XRD analysis (Fig. 2). The crystalline peaks at 2θ = 26°, 32°, 33°, 34°, and 40° confirmed the formation of HAP structure [21,22]. As the OH^- ions are partially substituted by the F^-, (300) and (202) peaks are shifted. *n*FHAP and *n*FAP are compared with standard card of fluorapatite (JCDP #15–0876) and there is a good match with the standard both in terms of relative intensity and the position of the peaks [23].

Fig. 3 shows the FT-IR spectrum of the synthetic *n*HAP, *n*FHAP, and *n*FAP samples. The peaks at 1,096, 1,037, and 961 cm^{-1} must be due to the phosphate stretching vibration and the bands observed at 605, 570, and 471 cm^{-1} belong to the phosphate bending vibration [24–26]. The spectrum of the *n*HAP sample clearly shows bands corresponding to structural hydroxyl groups at 632 and 3,572 cm^{-1}, suggesting fluoride substitution for OH^- groups for the other samples [27]. Also the bands at 744 and 740 cm^{-1} in the spectra of *n*FHAP and *n*FAP samples are, respectively assigned to the O–H···F group [28]. The weak absorption bands at 871, 1,408, and 1,456 cm^{-1} are corresponding to vibrations of the carbonate groups, which might come from the atmospheric carbon dioxide while dissolving, stirring, reaction and the calcining processes [29,30]. The broad peaks at 1,640 cm^{-1} and 3,450 cm^{-1} are due to adsorbed water [31]. As is shown in Fig. 4, the appearance of new band at 743 cm^{-1} in fluoride treated n-HAP confirms the formation of O–H···F bond as reported in precious work [17,18]. And a vibration band appears at 760 cm^{-1} (Fig. 5) after fluoride treated *n*FAP which is attributed to F···H···F hydrogen bond [32,33].

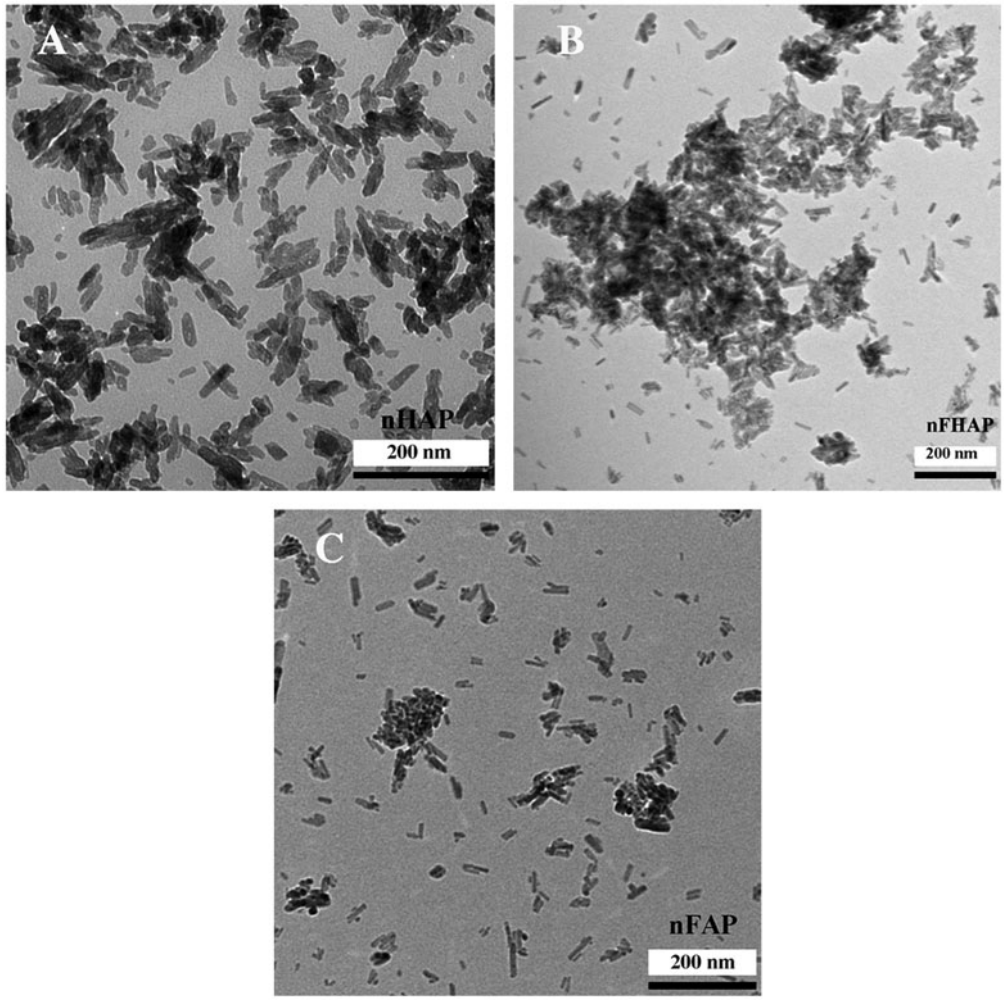

Fig. 1. TEM micrographs of the synthetic *n*HAP (A), *n*FHAP (B), *n*FAP (C).

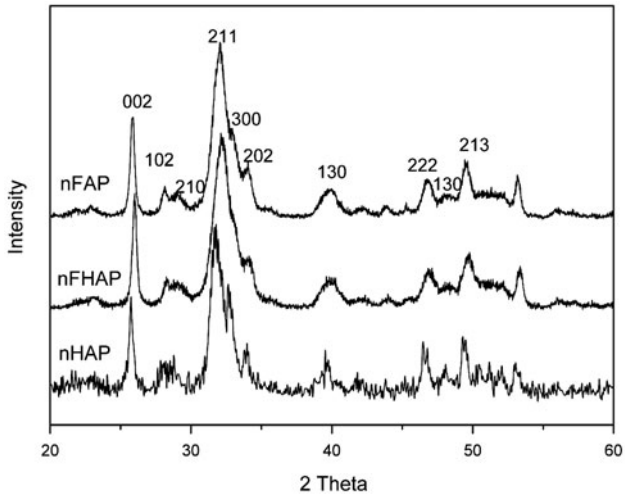

Fig. 2. XRD patterns of *n*HAP, *n*FHAP, and *n*FAP.

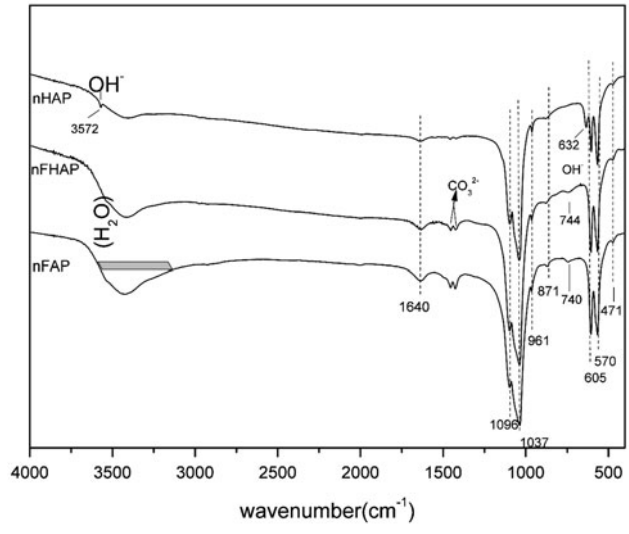

Fig. 3. FTIR spectra of *n*HAP, *n*FHAP, and *n*FAP.

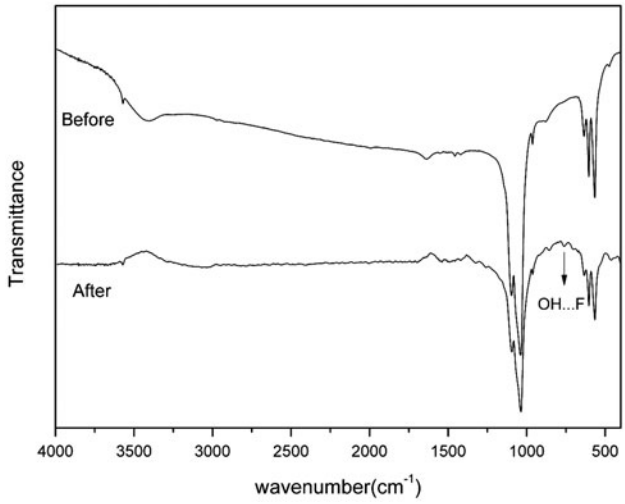

Fig. 4. FTIR spectra of *n*HAP before and after the adsorption of fluoride.

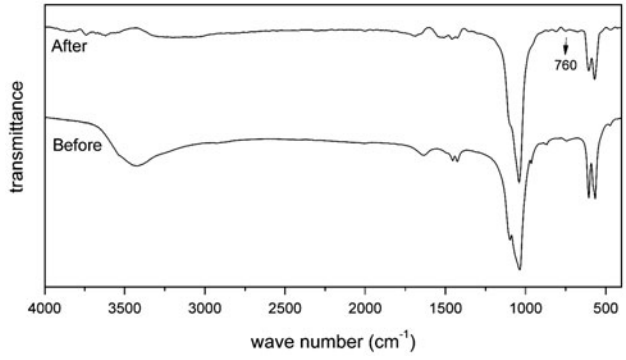

Fig. 5. FTIR spectra of *n*FAP before and after the adsorption of fluoride.

3.2. Effect of adsorbent dosage and contact time

The sorption of fluoride ion on adsorbents (*n*HAP, *n*FHAP, and *n*FAP) has been investigated of contact time in the range of 0–180 min with 10 mg/L as initial fluoride concentration at pH 5.0, room temperature (25˚C). The removal efficiency with contact time is shown in Fig. 6. The adsorption occurred in two steps: the adsorption process was fast in the first 30 min and a slower second phase which continued until the end of the experimental period. The equilibrium was established almost after 120 min and no remarkable changes were observed for longer contact time. The change in the rate of removal might be due to the fact that initially all adsorbent sites were vacant and the solute concentration gradient was high [34]. A contact time of 120 min was selected for further studies.

The adsorption of fluoride ion on adsorbents (*n*HAP, *n*FHAP, *n*FAP) has been investigated at pH

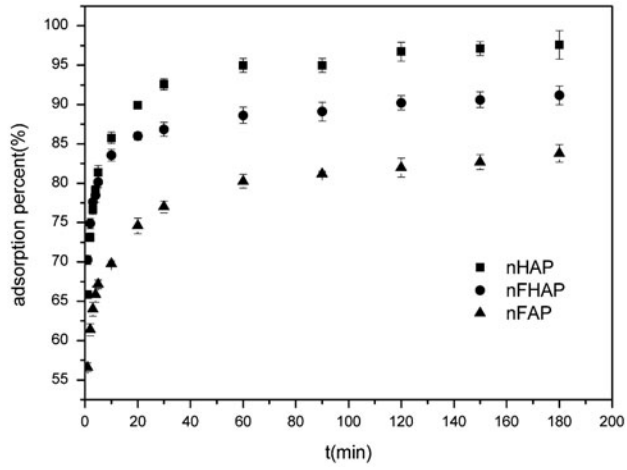

Fig. 6. Effect of contact time on fluoride removal by *n*HAP, *n*FHAP, and *n*FAP (adsorption conditions: pH = 5.0, initial fluoride concentration = 10 mg/L, adsorbent dose = 0.1 g/25 mL, and temperature = 25˚C).

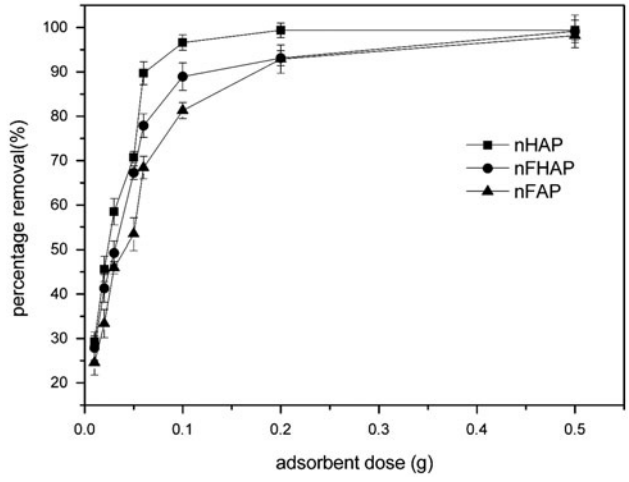

Fig. 7. Effect of adsorbent dose on fluoride removal percent by *n*HAP, *n*FHAP, and *n*FAP (adsorption conditions: pH = 5.0, initial fluoride concentration = 10 mg/L, contact time = 120 min, and temperature = 25˚C).

5.0 and contact time of 120 min with 10 mg/L as initial fluoride concentration at room temperature. As is shown in Figs. 7 and 8, adsorbent dosage was increased from 0.01 to 0.5 g/25 mL. It was obvious that with the addition of adsorbent dosage, the fluoride removal percentage increased, while the amount of fluoride loaded per unit weight of sorbent gradually decreased. Similar results had also been reported by other researchers [13,18]. With the increase in three materials dosage from 0.01 to 0.2 g/25 mL, the fluoride adsorption percent increased rapidly to more than 90%. This phenomenon could be

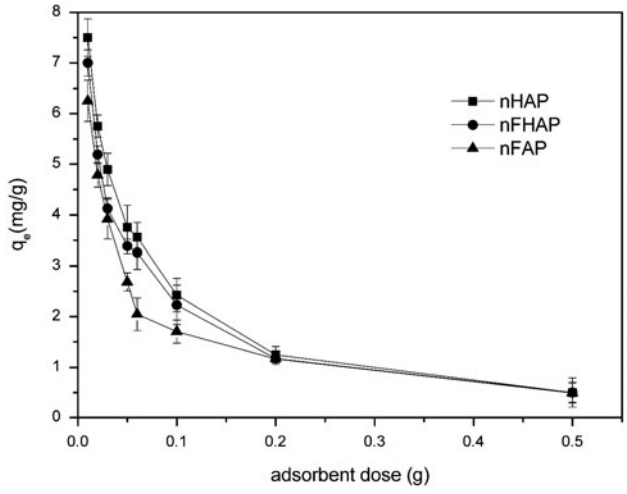

Fig. 8. Effect of adsorbent dose on adsorption of fluoride by *n*HAP, *n*FHAP, and *n*FAP (adsorption conditions: pH = 5.0, initial fluoride concentration = 10 mg/L, contact time = 120 min, and temperature = 25°C).

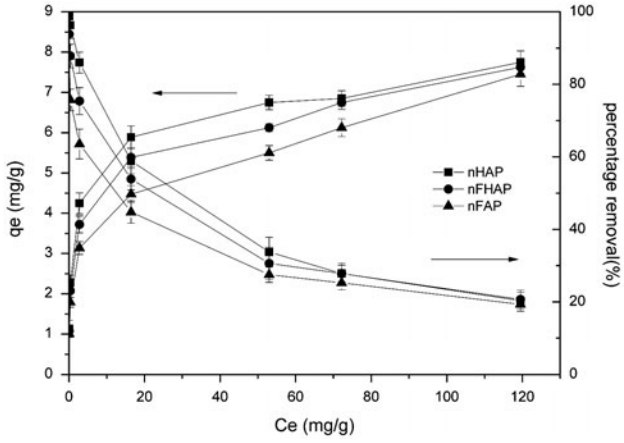

Fig. 9. Effect of equilibrium concentration on fluoride removal by *n*HAP, *n*FHAP, and *n*FAP (adsorption conditions: pH = 5.0, adsorbent dose = 0.1 g/25 mL, contact time = 120 min, and temperature = 25°C).

explained by the addition of per unit mass of the adsorbents caused the increase of the adsorption sites. But, as the dosage exceeded by 0.2 g/25 mL, the fluoride adsorption percentage just increased slightly and the removal efficiency reached nearly 100% with the dosage of 0.5 g/25 mL of the three materials, which also indicated that it was possible to remove fluoride completely when there was sufficient *n*FAP surface area in solution. On the other hand, the adsorption capacity showed that it was high at low dosages and reduced at high dosages. The main factor was that adsorption sites remain unsaturated during adsorption reaction, which was due to the fact that as the dosage of adsorbent was increased, there was less commensurate increase in adsorption resulting from the lower adsorptive capacity utilization of the adsorbent [35,36]. This leads to the conclusion that the available adsorption sites number increases by increasing the adsorbent dose and it, therefore, results in the increase of the amount of adsorbed fluoride ions. The decrease in equilibrium uptake with increase in the adsorbent dose is mainly because of unsaturation of adsorption sites through the adsorption process. The optimum dosage of 0.1 g/25 mL was chosen for further studies.

3.3. Effect of initial fluoride concentration

The equilibrium adsorption capacity (q_e) and adsorption percent (%) of fluoride adsorbed at varying initial fluoride concentration keeping other parameters content is presented in Fig. 9. It was clear to see that the q_e values increased while the percentage removal decreased with increasing initial fluoride concentrations. As the initial fluoride concentrations increased from 5 to 150 mg/L, for *n*HAP, the corresponding removal percentage decreased from 98.7 to 22.3% gradually. For *n*FHAP, the corresponding removal percentage decreased from 93.8 to 20.7% and for *n*FAP, decreased from 87.7 to 19.3%. The decrease of the removal percentage could be explained that the adsorbent offers a limited number of surface binding sites. The adsorption capacity of *n*HAP, *n*FHAP, and *n*FAP were 7.75, 7.625, and 7.45 mg/g for 150 mg/L initial fluoride concentrations, respectively. Results showed that the defluoridation efficiency of *n*FAP was as high as *n*HAP and the adsorption of fluoride by *n*FAP was attributed to F···H···F hydrogen bond as indicated by the FTIR analysis.

3.4. Effect of pH

It is well known that the pH of the aqueous solution plays an important role which controls the adsorption at the water adsorbent interface. Therefore, the adsorptions of fluoride were examined at initial pH values of 3.0, 4.0, 5.0, 6.0, 7.5, 9.0, and 10.5 by adding sufficient HCl/NaOH solution with 10 mg/L as initial fluoride concentration at room temperature, and the removal percent and final pH were plotted in Fig. 10. It could be inferred that the fluoride removal decreases with the increasing pH. The maximum fluoride removal was achieved at pH 3.0 and the minimum was at pH 10.5. At pH 3.0, the maximum defluoridation capacity of adsorbents (*n*HAP, *n*FHAP, and *n*FAP) was recorded as 2.47, 2.41, and 2.36 mg F^-/g, respectively. At very lower pH values, the

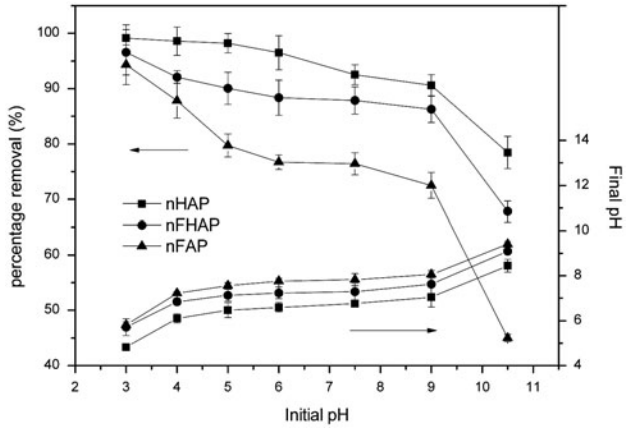

Fig. 10. Effect of pH on fluoride removal by *n*HAP, *n*FHAP, and *n*FAP (adsorption conditions: initial fluoride concentration = 10 mg/L, adsorbent dose = 0.1 g/25 mL, contact time = 120 min, and temperature = 25°C).

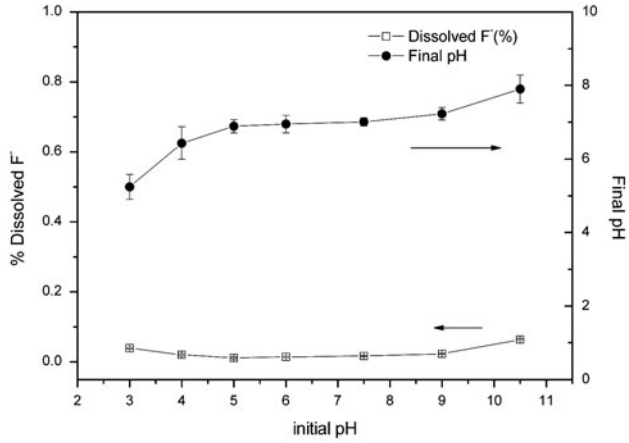

Fig. 11. Effect of pH on the dissolution of *n*FAP (dissolved conditions: adsorbent dose = 0.1 g/25 mL, contact time = 180 min, and temperature = 25°C).

surface of the adsorbents will be surrounded by the hydrogen ions which enhance the fluoride adsorption through electrostatic attraction, however, at high pH values of alkaline, lower adsorption capacity of fluoride can be explained by the fact that the surface acquires negative charge in alkaline pH, and hence there is a repulsion between the negatively charged surface and fluoride [18]. Moreover, at low pH, a hydrogen bonding mechanism plays an important role in defluoridation and the removal of fluoride is pretty good with all the adsorbents. On the other hand, with the increase of pH value, the hydrogen bond is so weak that it is easily broken, which could also decrease the adsorption of fluoride.

Fig. 11 shows the percentage of the fluoride concentration in *n*FAP with 0.1 g *n*FAP dissolution in 25 ml pure water after a transient time of 180 min. Release of fluorine from the *n*FAP structure into solution was observed for systems with initial pH of 3.0, 4.0, 5.0, 6.0, 7.5, 9.0, and 10.5. Dissolved concentrations of fluorine showed that less than 0.1% of the *n*FAP was solubilized indicated that there was no environmental threat about dissolved fluoride in *n*FAP.

3.5. Adsorption isotherms

The adsorption isotherms express the specific relation between the concentration of sorbate and its degree of accumulation onto the adsorbent surface at constant temperature. The two most commonly used isotherms, named Langmuir and Freundlich isotherms have been adopted [37].

The Langmuir theory is valid for monolayer adsorption onto a surface containing a finite number of identical sites and is one of the most popular isotherm models due to its simplicity and its good agreement with experimental data. The Langmuir isotherm equation is expressed in the linear form as:

$$\frac{1}{q_e} = \frac{1}{Q_0} + \frac{1}{Q_0 K_L C_e}$$

where q_e (mg/g) is the amount adsorbed at equilibrium; C_e (mg/L) is the equilibrium concentration of fluoride in solution; Q_0 (mg/g) is the maximum monolayer adsorption capacity; and K_L (L/mg) is the constant related to the free energy of adsorption. A linear plot is obtained for the sorbent when $1/q_e$ is plotted against $1/C_e$ which gives Q_0 and K_L values from the slope and intercept, respectively and the calculated results are listed in Table 2.

The Freundlich isotherm model is an empirical equation and the model is valid for heterogeneous surfaces. It assumes that the adsorption process occurs on the heterogeneous surfaces and the adsorption capacity is related to the concentration of phenol at equilibrium. The Freundlich model is generally expressed in linear form as:

$$\ln q_e = \ln K_F + \frac{1}{n} \ln C_e$$

where q_e (mg/g) is the amount adsorbed at equilibrium; K_F [mg/g (L/mg)], is the empirical constant of Freundlich isotherm; The constant n is the empirical parameter related to the intensity of adsorption, which varies with the heterogeneity of the material. When $1/n$ values are in the range $0.1 < 1/n < 1$, the

adsorption process is favourable. C_e (mg/L) is the equilibrium concentration of the fluoride in solution. The Freundlich model contents K_F and n are calculated from the slope and intercept of the plot of ln q_e vs. ln C_e, and the calculated results are listed in Table 2.

Table 2 summarizes the contents of the Langmuir and Freundlich constants. Most of the R^2 values exceed 0.9 for both the Freundlich and Langmuir models, suggesting that both the models closely fitted the experimental results. The adsorption capacity (measured by K_F) is: *n*HAP (0.658 L/mg) > *n*FHAP (0.575 L/mg) > *n*FAP (0.497 L/mg). The K_F value of sample HAP is greatest in comparison with that of others and therefore the adsorption capacity is the largest. The constant n is the empirical parameter related to the intensity of adsorption, which varies with the heterogeneity of the material. All values of n exceed one, suggesting the adsorptions of fluoride onto *n*HAP, *n*FHAP, and *n*FAP are physical process. The value of $1/n$ lies between 0 and 1 and the n value lying in the range of 1 to 10 confirms the favorable conditions for adsorption [38–40]. The Freundlich exponent $1/n$ between 0.5283 and 0.5558 indicates favorable adsorption and a high affinity of *n*HAP, *n*FHAP, and *n*FAP for fluoride. Values of q_m, defined as the maximum capacity of adsorbents, have been calculated from the Langmuir plots. The maximum adsorption capacity (measured by q_m) is: *n*HAP (11.75 mg/g) > *n*FHAP (10.74 mg/g) > *n*FAP (9.71 mg/g). K_L lied between zero and one, suggesting that the adsorptions of fluoride on three absorbents are favorable.

In summary, this section study showed that the adsorptions of fluoride onto the three adsorbents were fitted well with the equation Langmuir compared to Freundlich equation, according to the R^2 values shown in Table 2.

3.6. Adsorption kinetics studies

In order to investigate the sorption mechanism of fluoride removal, pseudo-first-order [41] and pseudo-second-order kinetic models [42] have been used at different experimental conditions.

Pseudo-first-order model:

$$\log(q_1 - q_t) = \log q_1 - \frac{K_1 t}{2.303}$$

Pseudo-second-order model:

$$\frac{t}{q_t} = \frac{1}{k_2 q_2^2} + \frac{t}{q_2}$$

where q_t (mg/g) is the uptake of fluoride at time t, t (min) is the shaken time, q_1 (mg/g) is the maximum adsorption capacity for pseudo-first-order, and K_1 (min^{-1}) is the pseudo-first-order rate constant for fluoride in adsorption process, respectively. And q_2 (mg/g) is the maximum adsorption capacity for pseudo-second-order. K_2 (g/(mg min)) is the pseudo-second-order rate constant for fluoride in adsorption process. The linear plots of fluoride adsorption kinetics to the two models and the calculated kinetic parameters are given in Table 3.

The R^2 was applied to determine the relationship between the experimental data and the kinetics in most studies. It is clear to see that the R^2 value for the pseudo-second-order kinetic model is much higher than those for the first-order kinetic model. For *n*HAP, *n*FHAP, and *n*FAP samples, the R^2 of the pseudo-second-order kinetic model are 0.9998, 0.9997, and 0.9997. Also, the calculated equilibrium capacity calculated from the pseudo-second-order model is in close agreement with the experimentally determined value. Therefore, the pseudo-second-order model is the better choice to describe the adsorption behavior of fluoride.

3.7. Thermodynamic parameters

The thermodynamic parameters, such as standard free energy change (ΔG°), enthalpy change (ΔH°), and entropy change (ΔS°) of adsorption were calculated using the following equations [43]:

Table 2
Parameters of adsorption isotherms of fluoride on *n*HAP, *n*FHAP, and *n*FAP at temperature 25°C

Sample	Langmuir			Freundlich		
	q_m (mg/g)	K_L (L/mg)	m	$1/n$	K_F (L/mg)	R^2
*n*HAP	11.75	0.268	0.9871	0.528	0.658	0.9064
*n*FHAP	10.74	0.233	0.9939	0.549	0.575	0.9399
*n*FAP	9.71	0.226	0.9991	0.556	0.497	0.9672

Table 3
Lagergren constants for the adsorption of fluoride onto *n*HAP, *n*FHAP, and *n*FAP at temperature 25°C

Sample	Pseudo-first-order rate contents			Pseudo-second-order rate contents		
	q_1 (mg/g)	K_1 (g/mg min^{-1})	R^2	q_2(mg/g)	K_2 (g/mg min^{-1})	R^2
*n*HAP	0.979	0.776	0.7042	2.458	0.293	0.9998
*n*FHAP	0.978	1.182	0.9098	2.252	0.486	0.9997
*n*FAP	0.975	0.704	0.9265	2.126	0.276	0.9997

$$\Delta G^\circ = -RT \ln K_c$$

The apparent equilibrium constant (K_c) of the adsorption is defined as [41]:

$$K_c = \frac{C_{ad,eq}}{C_{eq}}$$

where $C_{ad,eq}$ and C_{eq} are the concentration of fluoride on the adsorbent and residual fluoride concentration at equilibrium, respectively.

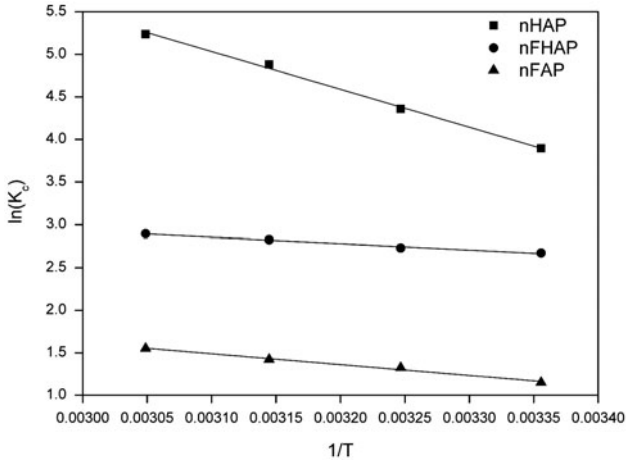

Fig. 12. $\ln(q_e/C_e)$ vs. $1/T$ for the adsorption of fluoride from aqueous solution.

$$\ln k_c = \frac{\Delta S^\circ}{R} - \frac{\Delta H^\circ}{RT}$$

where ΔG° (J) is standard free energy change; R (8.314 Jmol^{-1} K^{-1}) is the universal gas constant [44,45].

The values of ΔH° and ΔS° have been computed from the slope and intercept of the straight line of plots of log (q_e/C_e) vs. $1/T$ (Fig. 12). The values of these thermodynamic properties are given in Table 4. The results indicate that ΔG° values are negative which mean that the reaction is spontaneous. The free energy of the process at all temperatures was negative and changed with the rise in temperature. Positive values of ΔH° indicate the endothermic nature of the adsorption process. This suggests that with the increasing temperature, the adsorption capacity also increases. The positive ΔS° values for the present system show that randomness increases at the solid/solution interface during the adsorption of fluoride onto *n*HAP, *n*FHAP, and *n*FAP.

3.8. Regeneration of adsorbents

To make a cost-effective and user-friendly process, the adsorbent should be regenerated, so as to reuse for further fluoride adsorption. The regeneration effects of *n*HAP, *n*FHAP, and *n*FAP depend on the proportion, which is the ratio of adsorption capacity regenerated to the first adsorption capacity and the greater of the percentage, the better of the effect of the regeneration. It is apparent that all of the absorbents can be regenerated very well by the NaOH concentra-

Table 4
Thermodynamic parameters obtained at different temperatues for fluoride adsorption onto *n*HAP, *n*FHAP, and *n*FAP

	ΔS (J/mol K)	ΔH (kJ/mol)	ΔG (kJ/mol)			
			25°C	35°C	45°C	55°C
*n*HAP	156.45	3.697	−9.655	−11.156	−12.907	−14.281
*n*FHAP	42.7664	6.139	−6.6245	−6.997	−7.471	−7.894
*n*FAP	45.4079	10.642	−2.850	−3.395	−3.764	−4.237

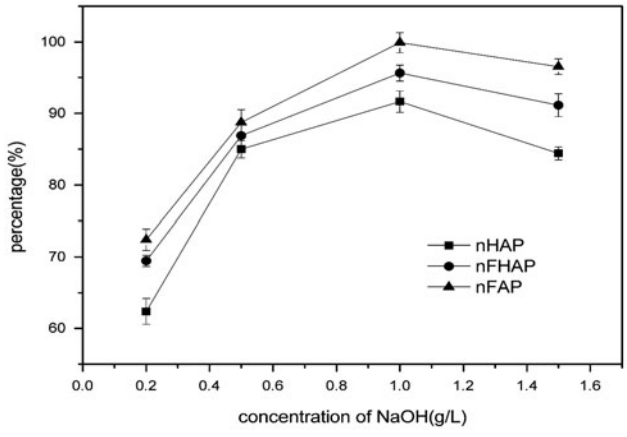

Fig. 13. Regeneration percentage of the adsorbents.

tion of 1.0 g/L as seen in Fig. 13, especially for FHA which is almost regenerated completely. With the same range of NaOH concentration, the regeneration capacity of *n*FAP appears to perform better. That could be explained that the more difficult adsorption of an adsorbent, the better performance it appears on regeneration. The maximum fluoride adsorption capacity of *n*FAP was similar to that of *n*HAP, and *n*FAP had lower cost and could be regenerated easily than *n*HAP, therefore *n*FAP had great potential in the removal of fluoride from aqueous solution.

4. Conclusion

The *n*FAP produced in this work were found to be effective in the removal of fluoride from aqueous solution. The adsorption of fluoride by *n*FAP was fast and reached equilibrium in 120 min of contact time. Increase in the initial fluoride concentration could effectively increase the fluoride adsorption capacity. Meanwhile, increase in the adsorbent dosage could effectively increase the fluoride removal percent. However, the adsorption capacity decreased continuously with the increase of solution pH. The maximum fluoride adsorption capacity was obtained as 7.45 mg/g for 150 mg/L initial fluoride concentrations at pH 5.0 and 25℃ for *n*FAP, which is similar to that of *n*HAP, and *n*FAP has advantages including lower cost and easy regeneration property, which make it a very promising adsorbent for the removal of fluoride from aqueous solution.

Acknowledgments

This work is supported by the National Programs for High Technology Research and Development of China (No. 2007AA10Z406), the Research Fund for the Doctoral Program of Higher Education (No. 20113207110014), SRF for ROCS, SEM, the Foundation for Talent Recommendation Program of Nanjing Normal University (No. 2009103XGQ0063 and No. 2011105XGQ0247), Program of Natural Science Research of Jiangsu Higher Education Institutions of China (No. 12KJB610002), and PAPD (a project funded by the Priority Academic Program Development of Jiangsu Higher Education Institutions).

References

[1] M. Hichour, F. Persin, J. Sandeaux, C. Gavach, Fluoride removal from waters by Donnan dialysis, Sep. Purif. Technol. 18 (2000) 1–11.
[2] P.Y. Zhu, H.Z. Wang, B.W. Sun, P.C. Deng, S.Q. Hou, Y.W. Yu, Adsorption of fluoride from aqueous solution by magnesia-amended silicon dioxide granules, J. Chem. Technol. Biotechnol. 84 (2009) 1449–1455.
[3] S.K. Swain, T. Padhi, T. Patnaik, R.K. Patel, U. Jha, R.K. Dey, Kinetics and thermodynamics of fluoride removal using cerium-impregnated chitosan, Desalin. Water Treat. 13 (2010) 369–381.
[4] Y. Vijaya, S.R. Popuri, G.S. Reddy, A. Krishnaiah, Development and characterization of chitosan coated biopolymer sorbent for the removal of fluoride ion from aqueous solutions, Desalin Water Treat. 25 (2011) 159–169.
[5] Y. Zhou, C. Yu, Y. Shan, Adsorption of fluoride from aqueous solution on La^{3+}-impregnated cross-linked gelatin, Sep. Purif. Technol. 36 (2004) 89–94.
[6] K.M. Popat, P.S. Anand, B.D. Dasare, Selective removal of fluoride ions from water by the aluminium form of the aminomethylphosphonic acid-type ion exchanger, React. Polym. 23 (1994) 23–32.
[7] S. Meenakshi, N. Viswanathan, Identification of selective ion exchange resin for fluoride sorption, J. Colloid Interface Sci. 308 (2007) 438–450.
[8] S. Saha, Treatment of aqueous effluent for fluoride removal, Water Res. 27 (1993) 1347–1350.
[9] R. Aldaco, A. Irabien, P. Luis, Fluidized bed reactor for fluoride removal, J. Chem. Eng. 107 (2005) 113–117.
[10] A.J. Karabelas, S.G. Yiantsios, Z. Metaxiotou, N. Andritsos, A. Akiskalos, G. Vlachopoulos, S. Stavroulias, Water and materials recovery from fertilizer industry acidic effluents by membrane processes, Desalination 138 (2001) 93–102.
[11] N. Drouiche, H. Lounici, M. Drouiche, N. Mameri, N. Ghaffour, Removal of fluoride from photovoltaic wastewater by electrocoagulation and products characteristics, Desalin Water Treat. 7 (2009) 236–241.
[12] G.E. Jai Poinern, M.K. Ghosh, Y.J. Ng, T.B. Issa, S. Anand, P. Singh, Defluoridation behavior of nanostructured hydroxyapatite synthesized through an ultrasonic and microwave combined technique, J. Hazard. Mater. 185 (2011) 29–37.
[13] S. Gao, J. Cui, Z.G. Wei, Study on the fluoride adsorption of various apatite materials in aqueous solution, J. Fluorine Chem. 130 (2009) 1035–1041.
[14] M. Jiménez-Reyes, M. Solache-Ríos, Sorption behavior of fluoride ions from aqueous solutions by hydroxyapatite, J. Hazard. Mater. 180 (2010) 297–302.
[15] C.S. Sundaram, N. Viswanathan, S. Meenakshi, Defluoridation chemistry of synthetic hydroxyapatite at nano scale: Equilibrium and kinetic studies, J. Hazard. Mater. 155 (2008) 206–215.
[16] S. Gao, R. Sun, Z.G. Wei, H.Y. Zhao, H.X. Li, F. Hu, Size-dependent defluoridation properties of synthetic hydroxyapatite, J. Fluorine Chem. 130 (2009) 550–556.
[17] Y. Wang, N.P. Chen, W. Wei, J. Cui, Z.G. Wei, Enhanced adsorption of fluoride from aqueous solution onto nanosized hydroxyapatite by low-molecular-weight organic acids, Desalination 276 (2011) 161–168.

[18] C.S. Sundaram, N. Viswanathan, S. Meenakshi, Uptake of fluoride by nano-hydroxyapatite/chitosan, a bioinorganic composite, Biores. Technol. 99 (2008) 8226–8230.
[19] G.W.C. Silva, L. Ma, O. Hemmers, D. Lindle, Micro-Structural characterization of precipitation-synthesized fluorapatite nano-material by transmission electron microscopy using different sample preparation techniques, Micron 39 (2007) 269–274.
[20] Y.M. Chen, X.G. Miao, Effect of fluorine addition on the corrosion resistance of hydroxyapatite ceramics, Ceram. Int. 30 (2004) 1961–1965.
[21] J. Wei, Y.B. Li, Tissue engineering scaffold material of nano—apatite crystals and polyamide composite, J. Eur. Poly. 40 (2004) 509–515.
[22] S. Meski, H. Khireddine, S. Ziani, S. Rengaraj, M. Sillanpaa, Comparative study on the removal of zinc(II) by bovine bone, billy goat bone and synthetic hydroxyapatite, Desalin. Water Treat. 16 (2010) 271–281.
[23] M.H. Fathi, E.M. Zahrani, Fathi, Mechanical alloying synthesis and bioactivity evaluation of nanocrystalline fluoridated hydroxyapatite, J. Cryst. Growth 311 (2009) 1392–1403.
[24] W. Wei, R. Sun, Z.G. Wei, H.Y. Zhao, H.X. Li, F. Hu, Elimination of the interference from nitrate ions on oxalic acid in RP-HPLC by solid-phase extraction with nanosized hydroxyapatite, J. Liq. Chromatogr. Rel. Technol. 32 (2009) 106–124.
[25] J. Harrison, A.J. Melville, J.S. Forsythe, B.C. Muddle, A.O. Trounson, K.A. Gross, R. Mollard, Sintered hydroxyfluorapatites—IV: The effect of fluoride substitutions upon colonisation of hydroxyapatites by mouse embryonic stem cells, Biomaterials 25 (2004) 4977–4986.
[26] N. Rameshbabu, T.S.S. Kumar, K.P. Rao, Synthesis of nanocrystalline fluorinated hydroxyapatite by microwave processing and its *in vitro* dissolution study, Bull. Mater. Sci. 29 (2006) 611–615.
[27] G. Penel, G. Leroy, C. Rey, B. Sombret, J.P. Huvenne, E. Bres, Infrared and Raman microspectrometry study of fluor-fluorhydroxy and hydroxy-apatite powders, J. Mater. Sci. - Mater. Med. 8 (1997) 271–276.
[28] A. Laghzizil, N. Elhrech, O. Britel, A. Bouhaouss, M. Ferhat, Removal of fluoride from moroccan phosphate and synthetic fluoroapatites, J. Fluorine Chem. 101 (2000) 69–73.
[29] J. Liu, X, Ye, H, Wang, M. Zhu, B. Wang, H. Yan, The influence of pH and temperature on the morphology of hydroxyapatite synthesized by hydrothermal method, Ceramics Int. 29 (2003) 629–633.
[30] Y.J. Wang, J.D. Chen, K. Wei, S.H. Zhang, X.D. Wang, Surfactant-assisted synthesis of hydroxyapatite particles, Mater. Lett. 60 (2006) 3227–3231.
[31] J.K. Han, H.Y. Song, F. Saito, B.T. Lee, Synthesis of high purity nano-sized hydroxyapatite powder by microwave-hydrothermal method, Mater. Chem. Phys. 99 (2006) 235–239.
[32] M.A. Richard, J.K. Joseph, Infrared spectral studies of hydrogen bonding phenomena in solutions containing hydrogen fluoride, J. Mol. Spectrosc. 1 (1957) 306–332.
[33] R.K. Thomas, Hydrogen bonding in the vapour phase between water and hydrogen fluoride: the infrared spectrum of the 1:1 complex, Proc. R. Soc. Lond. A344 (1975) 579–592.
[34] P. Gaurang, P. Usha, M. Shobhana, Removal of Fluoride from Aqueous Solution by CaO Nanoparticles, Sep. Sci. Technol. 44 (2009) 2806–2826.
[35] V.K. Gupta, I. Ali, V.K. Saini, Defluoridation of wastewaters using waste carbon slurry, Water Res. 41 (2007) 3307–3316.
[36] R.P. Han, W.H. Zou, Z.P. Zhang, J. Shi, J.J. Yang, Removal of copper (II) and lead(II) from aqueous solution bymanganese oxide coated sand. I. Characterization and kinetic study, J. Hazard. Mater. 137 (2006) 480–488.
[37] W.G. Kim, M.N. Kim, S.M.Lee, J.K.Yang, Removal of Cu(II) with hydroxyapatite (animal bone) as an inorganic ion exchanger, Desalin. Water Treat. 4 (2007) 269–273.
[38] K.L. Lin, J.Y. Pan, Y.W. Chen, R.M. Cheng, X.C. Xu, Study the adsorption of phenol from aqueous solution on hydroxyapatite nanopowders, J. Hazard. Mater. 161 (2009) 231–240.
[39] W. Wei, R. Sun, J. Cui, Z.G. Wei, Removal of nitrobenzene from aqueous solution by adsorption on nanocrystalline hydroxyapatite, Desalination 263 (2010) 89–96.
[40] T.Y. Hsien, Y.L. Liu, C.H. Huang, P.H. Lin, D.M. Wang, Synthesis of novel PVA crosslink mixed matrix scaffolds and adsorption of copper ions from waste water, Desalin. Water Treat. 34 (2011) 354–360.
[41] N. Das, P. Pattanaik, R. Das, Defluoridation of drinking water using activated titanium rich bauxite, J. Colloid Interface Sci. 292 (2005) 1–10.
[42] Y. Vijaya, M.V. Subbaiah, A.S. Reddy, A. Krishnaiah, Equilibrium and kinetic studies of fluoride adsorption by chitosan coated perlite, Desalin Water Treat. 25 (2011) 143–149.
[43] E.I. Unuabonah, K.O. Adebowale, B.I. Olu-Owolabi, Kinetic and thermodynamic studies of the adsorption of lead (II) ions onto phosphate-modified kaolinite clay, J. Hazard. Mater. 144 (2007) 386–395.
[44] M. Dundar, C. Nuhoglu, Y. Nuhoglu, Adsorption of Cu(II) ions onto the litter of natural trembling poplar forest, J. Hazard. Mater. 151 (2008) 186–195.
[45] A. Zach-Maor, R. Semiat, H. Shemer, Removal of heavy metals by immobilized magnetite nano-particles, Desalin. Water Treat. 31 (2010) 64–70.